Dynamic states of a continuum traffic equation with on-ramp

H. Y. Lee,[1,2] H.-W. Lee,[1] and D. Kim[1,2]

[1]*Center for Theoretical Physics, Seoul National University, Seoul 151-742, Korea*
[2]*Department of Physics, Seoul National University, Seoul 151-742, Korea*

We study the phase diagram of the continuum traffic flow model of a highway with an on-ramp. Using an open boundary condition, traffic states and metastabilities are investigated numerically for several representative values of the upstream boundary flux f_{up} and for the whole range of the on-ramp flux f_{rmp}. An inhomogeneous but time-independent traffic state (standing localized cluster state) is found and related to a recently measured traffic state. Due to the density gradient near the on-ramp, a traffic jam can occur even when the downstream density is below the critical density of the usual traffic jam formation in homogeneous highways, and its structure varies qualitatively with f_{rmp}. The free flow, the recurring hump (RH) state, and the traffic jam can all coexist in a certain metastable region where the free flow can undergo phase transitions either to the RH state or to the traffic jam state. We also find two nontrivial analytic solutions. These solutions correspond to the standing localized cluster state and the homogeneous congested traffic state (one form of the traffic jam), which are observed in numerical simulations. [S1063-651X(99)10405-7]

PACS number(s): 64.60.My, 89.40.+k, 05.40.−a

I. INTRODUCTION

Traffic flow, a many body system of strongly interacting vehicles, shows various complex behaviors. Numerous empirical data of the highway traffic have been obtained [1–5], which demonstrate the existence of distinct dynamic states and dynamic phase transitions between them. Recent studies reveal physical phenomena such as hysteresis, self-organized criticality, and phase transitions in the traffic flow [6,7].

The transition from the homogeneous free flow to the jammed state has been studied by microscopic and macroscopic models without any inhomogeneity in the system [8–14]. The traffic jam, one of the dynamic phases of the traffic flow, appears spontaneously when the vehicle density is between the two critical values ρ_{c1} and $\rho_{c2}(>\rho_{c1})$. The traffic jam, however, can appear even below ρ_{c1}. The traffic jam can be triggered by localized perturbations provided that the density is larger than a different critical value ρ_b ($<\rho_{c1}$). As a result, in the density range between ρ_b and ρ_{c1}, both the free flow and the traffic jam can exist, resulting in metastability and hysteresis [15–17]. It is observed that some features of the traffic jam are uniquely determined by underlying dynamics, and independent of initial conditions of the traffic flow that lead to the jam [4]. The presence of such characteristic features is also reproduced by analytic and numerical studies of traffic flow models [15,18].

The synchronized traffic flow, another dynamic phase of the traffic flow, is identified in recent measurements on highways [2,3]. The synchronized traffic flow resembles the traffic jam in the sense that both states produce inhomogeneous density and flow profiles. The dynamics of the synchronized flow is however much more complicated than that of the traffic jam. One notable property of the synchronized traffic flow is the high level of its average flow, which almost matches the flow of the free flow state. The synchronized traffic flow is observed, in nearly all occasions, localized near ramps and it is thus believed that ramps are important for the stability of the synchronized traffic flow. The discon-

tinuous transition from the free flow to the synchronized flow can be induced by localized perturbations of finite amplitudes. Measurements show a hysteresis effect in the phase transitions between the free flow and the synchronized flow: the transition from the synchronized flow to the free flow occurs at a lower on-ramp flux, or lower upstream flux, than that for the reverse transition. In Ref. [19], the recurring hump (RH) state is proposed as an origin of the (nonstationary type) synchronized traffic flow [3], and the dynamic phase transitions between the RH state and the free flow are investigated using continuum traffic equations that take into account the effect of ramps. In the RH state, the vehicle density and the velocity show temporal oscillations which are localized near on-ramps. That the synchronized flow is maintained for several hours can be explained from one important property of the RH state, its being a limit cycle of the traffic equations. The RH state can be characterized as a self-excited oscillator, where constant vehicle flux from an on-ramp serves as a source of the repeated excitation and each excitation is subsequently relaxed within a localized region. The traffic equations also describe the hysteresis phenomena between the RH state and the free flow.

The traffic jam and the synchronized traffic flow are distinct phases of traffic flow. However, the distinction between the conditions for the appearance of the jam state and the synchronized flow is not clearly identified yet, both in measurements and in model studies. Highway measurements analysis reports that almost identical initial states of the traffic flow can evolve to both the traffic jam and the synchronized flow [2].

To describe the hysteretic phase transitions between the free flow and the synchronized flow, a different macroscopic model based on a gas-kinetic approach is also proposed [20]. In this model, a peak of the inflow from an on-ramp produces a congested but homogeneous region near the on-ramp, which spreads in the upstream direction. This homogeneous congested traffic (HCT) state is proposed as an explanation for the (stationary type) synchronized traffic

flow [3]. The subsequent study [21] investigated the phase diagram of the model and identified additional dynamic phases such as the standing localized cluster (SLC), the triggered stop and go (TSG), and the oscillating congested traffic (OCT) states. Analytical conditions for the existence of these phases are provided and it is suggested that the phase diagram is universal for a class of traffic models. The study is, however, largely restricted to the traffic states generated from a particular initial condition and thus important issues such as multistability and hysteresis are not fully addressed.

In this paper, we investigate the phase diagram of the traffic flow in the presence of an on-ramp using a different continuum model [14], which tests the idea of the universal phase diagram. Various traffic states in Ref. [21] are reproduced. However, the phase diagram is found to be qualitatively different. For instance, some traffic states, which represent distinct phases in Ref. [21], make smooth crossovers to other traffic states without any sharp phase boundaries in between, implying that they are different limiting behaviors of a single dynamic phase. The investigation is also performed for a large variety of initial conditions using two effective search methods. The conditions for the stable existence of the free flow, the RH state, and the traffic jam are examined. In some parameter ranges, it is found that multiple dynamic phases can remain stable with respect to sufficiently small perturbations. In such parameter ranges, finite perturbations may induce transitions between those phases, resulting in metastability. Due to the presence of the on-ramp, the evolution process of the jam shows several different patterns and the phase boundaries for the formation of the jam are significantly modified.

The paper is organized as follows. In the next section, we investigate the possible traffic phases for given values of the upstream flux and the input flux through the on-ramp. Various features are discovered, which are absent in homogeneous highways. We examine the conditions for the stabilities of the traffic jam and the RH state. The metastability among the free flow, the RH state, and the traffic jam is investigated, and the travel time distributions of the three states are compared. We also discuss the several different evolution processes of the jam due to the presence of the on-ramp. Based on the phase diagrams, we find that the on-ramp flux becomes a more important factor for the formation of the traffic jam than the total flux, the sum of the on-ramp flux and the upstream flux. In Sec. III, we demonstrate analytically that our macroscopic model possesses nontrivial solutions which are indeed found in numerical simulations. Finally, Sec. IV summarizes our results.

II. PHASE DIAGRAMS OF TRAFFIC EQUATIONS WITH AN ON-RAMP

In this work, we adopt the continuum model of the highway traffic flow proposed by Kerner and Konhäuser [14],

$$\frac{\partial \rho}{\partial t} + \frac{\partial (\rho v)}{\partial x} = q_{in}(t)\varphi(x), \qquad (1)$$

$$\rho\left(\frac{\partial v}{\partial t} + v\frac{\partial v}{\partial x}\right) = \frac{\rho}{\tau}[V(\rho)-v] - c_0^2\frac{\partial \rho}{\partial x} + \mu\frac{\partial^2 v}{\partial x^2}, \qquad (2)$$

where $\rho(x,t)$ is the local vehicle density and $v(x,t)$ the local velocity. $q_{in}(t)\varphi(x)$ is the source term representing the external flux through an on-ramp. The spatial distribution of the external flux $\varphi(x)$ is localized near $x=0$ (on-ramp position) and normalized so that $q_{in}(t)$ denotes the total incoming flux. $V(\rho)$ is the safe velocity that is achieved in the time-independent and homogeneous traffic flow. In Eq. (2), the second term on the right hand side represents an effective ''pressure'' gradient on vehicles due to the anticipation driving [14] and the velocity fluctuations [5,13], and the third term takes into account an intrinsic dampening effect that is required to fit the experimental data [22]. Here τ, c_0, μ are appropriate constants. The flux or flow, ρv, is denoted below by either q or f.

In order to investigate the effects of a single on-ramp, we use the open boundary condition. The upstream boundary values of the density and velocity are fixed at $\rho(x=-L/2,t)=\rho_{up}$ and $v(x=-L/2,t)=V(\rho_{up})$, respectively. On the other hand, the values at the downstream boundary ($x=L/2$) are linearly extrapolated from their values at neighboring points, $x=L/2-\Delta x$ and $L/2-2\Delta x$ where Δx is spacing used in the discretization. The numerical simulations are performed using the two-step Lax-Wendroff scheme [23]. We choose the following parameters: $\tau=0.5$ min, $\mu=600$ vehicles km/h, $c_0=54$ km/h, and $V(\rho)=V_0(1-\rho/\hat{\rho})/(1+E(\rho/\hat{\rho})^4)$ where the maximum density $\hat{\rho}=140$ vehicles/km, $V_0=120$ km/h, and $E=100$ [24]. Concerning the discretization, spatial intervals of $\Delta x=37.8$ m and time intervals of $\Delta t=10^{-4}$ min are used. We choose the spatial distribution of the external flux as

$$\varphi(x)=(2\pi\sigma^2)^{-1/2}\exp(-x^2/2\sigma^2)$$

with $\sigma=56.7$ m. With this choice of parameters, critical values are $\rho_b=21.1$ vehicles/km, $\rho_{c1}=25.3$ vehicles/km, $\rho_{c2}=62.3$ vehicles/km, $f_b\equiv\rho_b V(\rho_b)=2047$ vehicles/h, $f_{c1}\equiv\rho_{c1}V(\rho_{c1})=2249$ vehicles/h, and $f_{c2}\equiv\rho_{c2}V(\rho_{c2})=843$ vehicles/h. The maximum flow that can be achieved in the time-independent homogeneous flow is $f_{max}=\max_\rho\{\rho V(\rho)\}=2336$ vehicles/h. Below we are interested mainly in the low density regime ($<\rho_{c1}$), and thus we will use for brevity the subscript c in place of $c1$.

In the real highway traffic, there are many kinds of noises which perturb the traffic out of its steady states. The real traffic state is hence under an infinite sequence of perturbations and subsequent responses of dynamic states. Previous studies [15,18] on highway traffic without ramps however showed that many observed features of the traffic flow can be explained from the steady state properties of the continuum model without any noise. Motivated by previous successes, we will ignore noises in this paper.

In the absence of noises, each dynamic phase of the traffic flow corresponds to a steady state, or equivalently an attractor of the nonlinear hydrodynamic model [Eqs. (1) and (2)]. A steady state may exhibit complicated time dependences depending on the nature of the corresponding attractor. We examine in this section the linearly stable steady states (or phases of traffic flow) for a given upstream flux $f(-L/2)=f_{up}\equiv\rho_{up}V(\rho_{up})$ and the vehicle flux $q_{in}(t)=f_{rmp}$ through the on-ramp at $x=0$. Linearly stable states are, however, often unstable to large perturbations and multistability can

occur. Here it is worth emphasizing that the concept of the multistability in dynamic systems is somewhat different from that in equilibrium systems. In equilibrium systems the free energy selects one particular state as a ''true'' stable state and other states become metastable. In dynamic systems, on the other hand, the free energy cannot be defined and the concept of the ''true'' stable state is not applicable. In this sense, all states are metastable and they all should be treated equally.

Possible presence of multiple steady states makes it very difficult to search completely for all phases that are stable for given parameters, since it requires examinations of many different initial conditions. To search out all multiple steady states, we use two methods: One is to apply a triggering pulse to a steady state, for example, by changing the value of f_{rmp} for a short time. For a sufficiently strong pulse, a transition to a different steady state can be induced, allowing the identification of another steady state. The other is the adiabatic sweeping method. Starting with a given steady state for a particular set of the system parameters, one increases or decreases one parameter adiabatically. This way, one can find the range of the parameter values where a dynamic state remains stable. These two methods effectively simulate a large variety of initial conditions. Using these, we investigate the steady states for given system parameters f_{up} and f_{rmp}. In particular, we concentrate on three representative values of f_{up}, and for each of them construct a phase diagram for the entire range of f_{rmp}. However, since too large a value of f_{rmp} is unrealistic, we restrict our attention to the range $f_{\text{rmp}} \leq f_{\text{rmp}}^{\text{max}} \equiv f_{\text{max}} - f_{\text{up}}$.

The values of f_{up} studied in this work are chosen from the following considerations. In the previous studies of homogeneous highways without ramps, it was found that the flux f_b provides an important boundary. Whereas the free flow is the only stable phase below f_b, the traffic jam can be created above this value. In the presence of ramps, one can expect that the appearance of the traffic jam depends on whether the upstream flux f_{up} is larger or smaller than f_b. (Below we show that this expectation is not true, due to the nontrivial effect of an on-ramp.) This property motivated us to choose one representative value of f_{up} in the range larger than f_b and another smaller. We also choose a very small value for $f_{\text{up}}(\ll f_b)$, which later reveals the importance of f_{rmp} on the formation of the congested traffic.

A. $f_{\text{up}} > f_b$

The phase diagram of the traffic states for $f_{\text{up}} = 2119$ vehicles/h appears in Fig. 1(a). Here f_{rmp}^c is the critical input flux through the on-ramp above which the free flow in the downstream of the on-ramp becomes linearly unstable. The critical on-ramp flux f_{rmp}^c is determined from

$$f_{\text{rmp}}^c = f_c - f_{\text{up}}, \tag{3}$$

where $f_c = f_{c1}$. For $0 \leq f_{\text{rmp}} \leq f_{\text{rmp}}^c$, the flux, both in the upstream and downstream, is lower than f_c but higher than f_b. Hence the traffic jam can be created from the free flow by triggering events but it does not appear spontaneously. The finite amplitude perturbation to f_{rmp} generates a cluster,
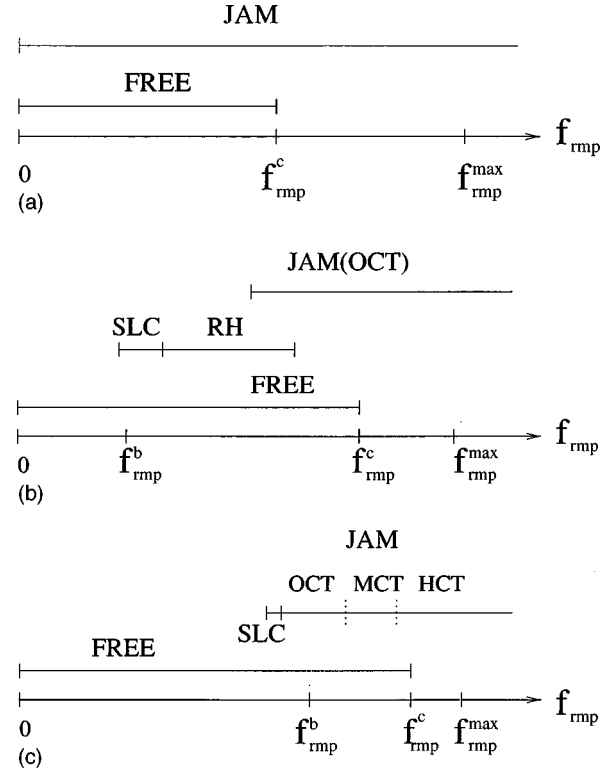

FIG. 1. The phase diagrams for $f_{\text{up}} > f_b$ (a), $f_{\text{up}} < f_b$ (b), and $f_{\text{up}} \ll f_b$ (c). Here $f_b = 2047$ vehicles/h, $f_c = 2249$ vehicles/h, and $f_{\text{max}} = 2336$ vehicles/h while $f_{\text{rmp}}^b \equiv f_b - f_{\text{up}}$, $f_{\text{rmp}}^c \equiv f_c - f_{\text{up}}$, and $f_{\text{rmp}}^{\text{max}} \equiv f_{\text{max}} - f_{\text{up}}$. (a) The phase diagram for $f_{\text{up}} = 2119$ vehicles/h where $f_{\text{rmp}}^c = 130$ vehicles/h, and $f_{\text{rmp}}^{\text{max}} = 217$ vehicles/h. For $f_{\text{rmp}} > f_{\text{rmp}}^c$, the traffic jam state is generated spontaneously. (b) The phase diagram for $f_{\text{up}} = 1948$ vehicles/h where $f_{\text{rmp}}^b = 99$ vehicles/h, $f_{\text{rmp}}^c = 301$ vehicles/h, and $f_{\text{rmp}}^{\text{max}} = 389$ vehicles/h. The metastable region among the free flow, the RH state, and the OCT state extends from $f_{\text{rmp}} = 206$ vehicles/h to 238 vehicles/h. (c) The phase diagram for $f_{\text{up}} = 1497$ vehicles/h where $f_{\text{rmp}}^b = 550$ vehicles/h, $f_{\text{rmp}}^c = 752$ vehicles/h, and $f_{\text{rmp}}^{\text{max}} = 839$ vehicles/h. As the on-ramp flux increases, the traffic jams with different structures appear. The lower stability limit of the HCT state is defined as the value of f_{rmp} above which the inhomogeneous part disappears. In a similar way, one may define the upper stability limit of the OCT as the value of f_{rmp} below which the homogeneous part does not expand with time. Notice that between these two stability limits, there exists an intermediate range of f_{rmp} for which both the OCT-like part (inhomogeneous part) and the HCT-like part (homogeneous part) expand with time. This intermediate state is called the ''mixed congested traffic'' (MCT) state. The stability limit between the OCT and MCT state is $f_{\text{rmp}} = 603$ vehicles/h and that between the MCT and HCT state is $f_{\text{rmp}} = 730$ vehicles/h.

which grows to a traffic jam since the upstream flux is larger than f_b. The traffic jam propagates to the upstream with its characteristic group velocity.

When $f_{\text{rmp}} > f_{\text{rmp}}^c$, the flux of the free flow in the downstream is larger than the critical flux f_c and the free flow is linearly unstable with respect to long wavelength perturbations of infinitesimal amplitude. The growth of infinitesimal perturbations leads to spontaneously formed clusters and as pointed out in Ref. [16], complex sequences of traffic jams may appear in the downstream region. In a certain range of f_{rmp}, we also observe that clusters form a periodic regular
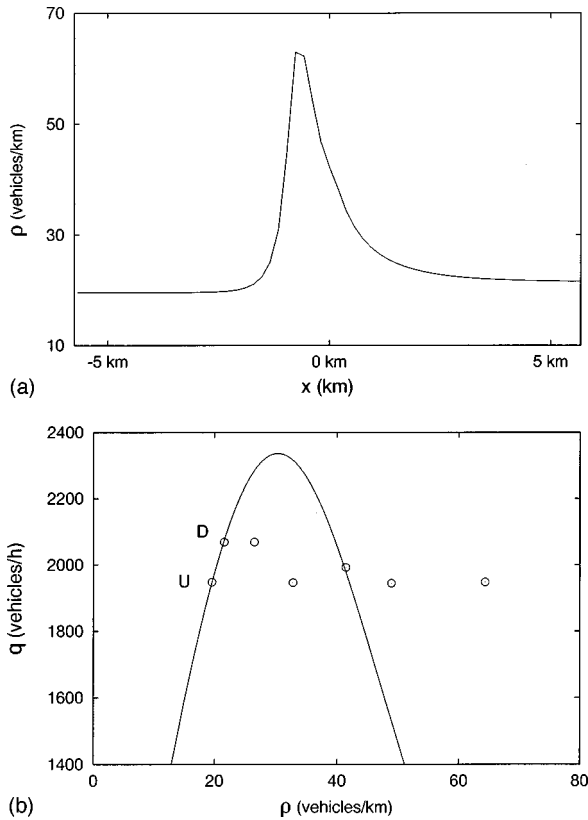
FIG. 2. (a) The spatial density profile of the SLC state for f_{up} = 1948 vehicles/h and f_{rmp} = 121 vehicles/h. The on-ramp is at 0 km. The profile does not change with time. (b) Circles: The density-flow relation for several positions near the on-ramp. That denoted as U(D) is the data in the upstream (downstream) homogeneous region. Each data point is stationary with time, and upon adiabatic variations of f_{up} and the external flux profile $\varphi(x)$, it covers a two-dimensional area. Solid line: The curve $q = \rho V(\rho)$.

sequence. It turns out that this regular sequence is caused by the presence of the on-ramp, whose detailed discussion will be given in the next subsection.

B. $f_{up} < f_b$

In Fig. 1(b), we present the phase diagram for f_{up} = 1948 vehicles/h. The free flow can exist until f_{rmp} reaches f_{rmp}^c, as in the previous subsection. When f_{rmp} is smaller than 92 vehicles/h, the free flow (with a transition layer) is the only stable phase.

For $f_{rmp} > 92$ vehicles/h, we find another time-independent state beside the free flow, which is shown in Fig. 2(a). In our simulation, this state can be generated from the free flow by applying the triggering pulse in f_{rmp} for a short time. Far away from the on-ramp, the density and flow are homogeneous both in the upstream and downstream. Near the on-ramp, a localized cluster appears, which does not propagate in either direction but stays motionless. Due to this immobility, such state is named as the "standing localized cluster" (SLC) state in Ref. [21]. The immobility of the SLC state is in contrast to the situations without ramps where all inhomogeneities should propagate. Hence the property is due to an effect of the on-ramp. Another interesting property of the SLC state becomes manifest in the density-flow rela-

tions. Notice that the density-flow relations [circles in Fig. 2(b)] measured at several locations near the on-ramp do not necessarily fall on the homogeneous density-flow relation curve $(\rho, \rho V(\rho))$ [solid line in Fig. 2(b)] even though the relation at each measurement location remains stationary with time. More remarkably, the circles lie in the linearly unstable density region.

Incidentally, an experimental data which may be relevant to this has been reported [3]. It was observed that when the traffic is in the stationary synchronized flow state, the density and flux can remain stationary during a relatively long time interval (2–5 min). Their stationary values often lie in the linearly unstable density region and they form a two-dimensional area in the density-flow plane instead of falling on a single well-defined density-flow relation curve. In Ref. [3], the stationary values are interpreted as an indication of the spatially *homogeneous* traffic, and Helbing, Hennecke, and Treiber [21] proposed the HCT state as an origin of the stationary synchronized flow. The HCT state provides an explanation for the stability of the traffic in the linearly unstable density region but it leads to the formation of the well-defined density-flow relation curve, failing to explain the absence of such a curve in the measurement.

Present analysis of the SLC state raises an alternative possibility. The SLC state shows that being stationary does not necessarily imply the homogeneity, and it also explains the stability in the linearly unstable density region. Furthermore it can explain the absence of the well-defined density-flow relation curve. We mention that upon the adiabatic variations of f_{up}, f_{rmp} and the external flux profile $\varphi(x)$, the density-flow relation at a single measurement location can cover a two-dimensional area in the density-flow plane. These agreements raises an interesting possibility of an alternative explanation for the stationary synchronized traffic flow based on the SLC state. We judge however that it is yet premature to draw a definite conclusion from these agreements alone. Further experimental investigation of the stationary synchronized traffic flow is necessary. In the next section, we demonstrate analytically that the traffic equations (1) and (2) do have the SLC state solution.

As the on-ramp flux f_{rmp} increases adiabatically, one finds the phase transition from the SLC state to the recurring hump (RH) state [Fig. 3(a)]. In the RH state, a cluster, or a hump, does not remain stationary but moves back and forth in a localized region near the on-ramp. Its drift to far upstream is not allowed since the upstream vehicle density is lower than the boundary value ρ_b. The RH state is investigated in detail in Ref. [19] using the periodic boundary condition, and many interesting properties are found such as the discontinuous transition from the free flow to the RH state induced by localized perturbations of finite amplitudes, hysteresis, gradual spatial transitions from the RH state to the free flow, and synchronized oscillations. These properties are identical to those of the synchronized flow (nonstationary type) [2,3], and based on these common properties, the RH state is proposed as the origin of the synchronized flow.

In addition to the properties of the RH state discussed in Ref. [19], we investigate here the transition between the RH state and the SLC state. Our simulation shows that the transition from the SLC state to the RH state and the reverse transition occur at the same critical value of f_{rmp} without
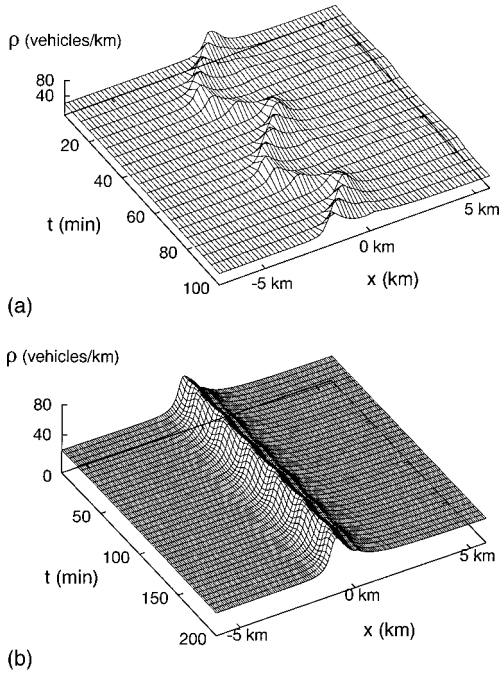
FIG. 3. (a) The evolution of the RH state for $f_{up}=1948$ vehicles/h and $f_{rmp}=222$ vehicles/h. The hump moves back and forth in a localized region near the on-ramp. (b) The evolution of the RH state for $f_{up}=1948$ vehicles/h and $f_{rmp}=130$ vehicles/h. Near the lower stability limit of the RH state, which coincides with the upper stability limit of the SLC state, the oscillation amplitude of the RH state is very small.
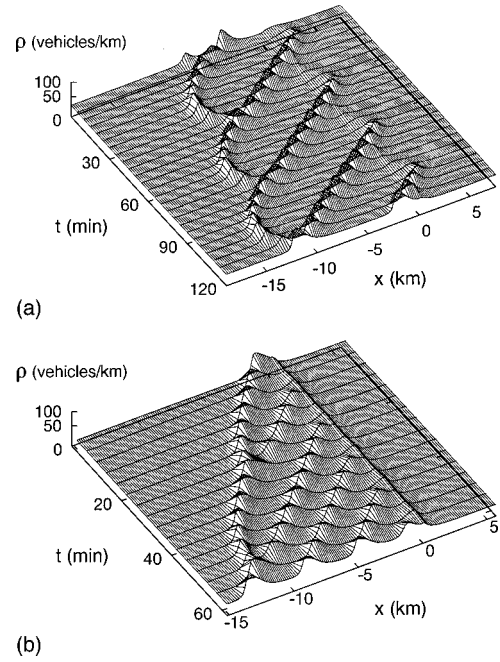

FIG. 4. (a) The spatiotemporal evolution of the density of the OCT state for $f_{up}=1948$ vehicles/h and $f_{rmp}=222$ vehicles/h. The values of f_{up} and f_{rmp} are the same with those in Fig. 3(a). The RH state in Fig. 3(a) and the OCT state in this figure are independent metastable states. (b) The spatiotemporal evolution of the OCT state for $f_{up}=1948$ vehicles/h and $f_{rmp}=381$ vehicles/h. The increase of f_{rmp} generates the ''closely packed'' clusters. Similarly to (a), each cluster decays at far upstream from the on-ramp.

hysteresis. We also examine the oscillation amplitude of the RH state. The amplitude decreases to zero continuously as f_{rmp} approaches the critical value [Fig. 3(b)]. Below the critical value, the hump does not oscillate and it becomes a standing cluster. These properties suggest that these transitions are a result of the supercritical (or very weak subcritical) Hopf bifurcation [25] of the SLC state to the RH state.

These transitions between the SLC state and the RH state are not observed in the previous study [19], where the adiabatic decrease of the ramp flux leads to the discontinuous transition of the RH state to the free flow instead (Fig. 3 in Ref. [19]). We attribute this difference to the different boundary condition adopted in this paper. Unlike the open boundary condition where f_{up} and f_{rmp} can be controlled independently, the periodic boundary condition used in [19] is such that the increase (decrease) of f_{rmp} is always accompanied by the decrease (increase) of f_{up} since the average density of the total system is fixed. Therefore the ''scanning'' direction in Ref. [19] is different from that in this paper.

We next discuss the traffic jam state. In homogeneous highways without ramps, the formation and propagation of the jam cannot occur when the flux is smaller than f_b. In the present case with an on-ramp, the flux f_{up} in the upstream region is lower than f_b while the flux in the downstream region can be controlled by f_{rmp}. Thus a usual jam that consists of a single localized cluster should decay after they reach the upstream region. So in this sense, a usual traffic jam is not a steady state. Our investigations show that a different type of traffic jams (Fig. 4) can occur even when $f_{up}<f_b$ due to the nontrivial effect of the on-ramp: Clusters

are self-generated near the on-ramp repeatedly, forming a ''train'' of clusters moving upstream. Although each constituting cluster decays during its upstream propagation, the train can still remain stable provided that the decay rate is smaller than the self-generation rate, which is controlled by the extent of the inhomogeneity, f_{rmp}, rather than by the upstream or downstream flux. Thus the stability limits of the new traffic jam do not coincide with those of the usual traffic jams [Fig. 1(b)]. Notice that this train structure is different from usual traffic jams in homogeneous highways. To indicate the structural difference, we will call this state the ''oscillating congested traffic'' (OCT) state.

We note that a traffic jam state very similar to the OCT state appears for $f_{up}>f_b$. Clusters are self-generated near the on-ramp repeatedly, forming a regular sequence of clusters. For $f_{up}>f_b$, however, each cluster does not decay in their upstream movement because of the high upstream density.

The structure of the OCT state can be compared to the RH state. In both states, clusters appear recurrently near the on-ramp. In the OCT state, however, the area of the congested region expands with time, while in the RH state, clusters are localized. This difference is due to the larger size of clusters in the former.

It is also worth mentioning that the structure of the OCT state shows an interesting crossover as f_{rmp} varies. For small values of f_{rmp} (close to the lower stability limit), the distance between the clusters is relatively large so that there exist homogeneous flow regions in between [Fig. 4(a)]. As f_{rmp} increases, the distance between the clusters shrinks and for
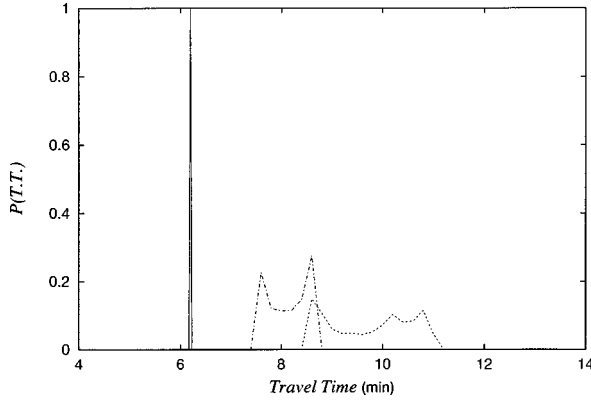
FIG. 5. The travel time distributions of the free flow (solid line), the RH state (dashed line), and the traffic jam (OCT) (dotted line) for $f_{up} = 1948$ vehicles/h and $f_{rmp} = 222$ vehicles/h. The travel time distributions are obtained by following 10^5 trajectories of vehicles through the region from -5 km to 5 km.

sufficiently large values of f_{rmp}, the homogeneous regions between them disappear [Fig. 4(b)], and the clusters are "closely packed" inside the congested region.

In Ref. [21], these structural differences are discovered using a different hydrodynamic model and the OCT states for small and large f_{rmp} are identified as two distinct phases. The former was called the "triggered stop and go" (TSG) flow and the latter OCT. In this paper, however, we find that these apparently different states transform smoothly to each other as f_{rmp} is varied, without any signature of singularities. Thus we group these two states as a single dynamic phase in this paper. This difference between this paper and Ref. [21] may be due to the different models used, but presently we do not know the precise origin of the difference.

We emphasize that in a certain range of f_{rmp}, three phases, the free flow, the RH state, and the traffic jam (OCT) can coexist. In this metastable region of f_{rmp}, small differences in the initial traffic condition may result in quite different final states. We mention that in a recent measurement [2], very similar initial states of the free flow are observed to undergo different phase transitions either to the synchronized flow or to the traffic jam. Here we obtain the three phases from the traffic equations with a fixed parameter set.

The difference between the three phases, the free flow, the RH state, and the traffic jam (OCT), is manifest in the travel time distributions which are shown in Fig. 5. In order to calculate the exact travel time distributions, we determine the trajectory of a vehicle, which is initially located at $x_{veh}(t_0)$, as follows:

$$x_{veh}(t) = x_{veh}(t_0) + \int_{t_0}^{t} dt' \ v(x_{veh}(t'), t'). \qquad (4)$$

From the trajectory of each vehicle, we obtain the vehicle travel time passing through the region from $x_0 = -5$ km to $x_1 = 5$ km. With the same $f_{up} = 1948$ vehicles/h and $f_{rmp} = 222$ vehicles/h, the travel time distributions of the three states show different behaviors. While it consists of a single peak for the free flow, those for the RH state and the traffic jam (OCT) show broad distributions due to the nonstationary

(a)
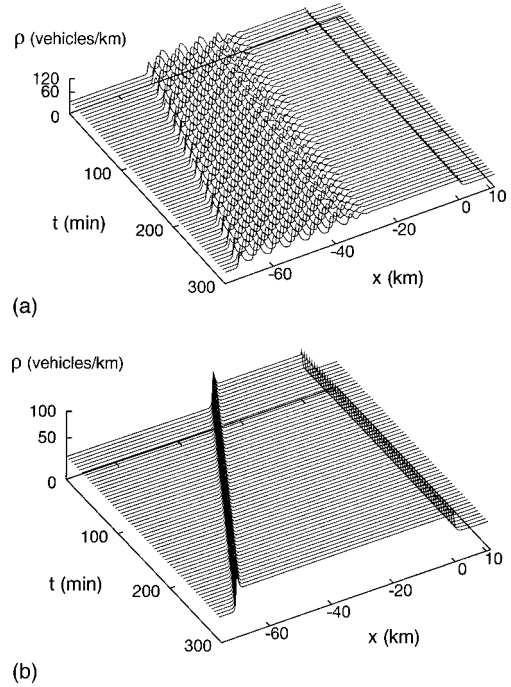

(b)

FIG. 6. The evolution of the MCT (a) and HCT state (b) for $f_{up} = 1497$ vehicles/h. (a) $f_{rmp} = 635$ vehicles/h. The congested region consists of the homogeneous part and the inhomogeneous part. (b) $f_{rmp} = 794$ vehicles/h. The inhomogeneous part is not present. The upstream front moves with a fixed group velocity.

nature of these phases. Also notice that in average, the travel time for the traffic jam (OCT) is greater than those for the free flow and the RH state.

C. $f_{up} \lesssim f_b$

Figure 1(c) shows the phase diagram for $f_{up} = 1497$ vehicles/h (about 25% lower than $f_b = 2047$ vehicles/h). The free flow remains linearly stable for $f_{rmp} < f_{rmp}^c$. In a narrow range of f_{rmp}, 480 vehicles/h $\leqslant f_{rmp} < 492$ vehicles/h, the SLC state is found, and for $f_{rmp} \geqslant 492$ vehicles/h, the OCT state is found. For this low upstream flux, however, the RH state does not appear. We find the critical value of f_{up} below the RH state is absent is about 1872 vehicles/h.

It is interesting to notice that the upper stability limit of the SLC state and the lower stability limit of the OCT state coincide within our numerical accuracy. We verified that upon the adiabatic increase of f_{rmp}, the SLC state undergoes the phase transition to the OCT state, and upon the adiabatic decrease of f_{rmp}, the reverse phase transition occurs, both at $f_{rmp} = 492$ vehicles/h. This coincidence raises an interesting possibility of a close relation between the two phases. This possibility is also supported by the expansion rate of the congested region, which seems to approach zero smoothly as f_{rmp} is reduced to the lower stability limit of the OCT state.

We next examine the evolution of the traffic jam state. Figure 6 shows the evolution of the structure of the congested region as f_{rmp} is increased. For relatively small f_{rmp}, the structure is the same as in Fig. 4. As f_{rmp} increases, however, a homogeneous flow region appears near the on-ramp, which expands with time [Fig. 6(a)]. Hence the congested region is partitioned into an inhomogeneous part and

a homogeneous one. For an even higher value of f_{rmp} ($=730$ vehicles/h), the inhomogeneous part shrinks in length with time and after this transient process, the whole congested region consists of a homogeneous part [Fig. 6(b)]. In Ref. [21], this state of traffic flow is named the ''homogeneous congested traffic'' (HCT) state and is identified as a distinct phase.

Unlike Ref. [21], however, it is not so clear in our simulations whether the OCT and HCT states are distinct phases. The distinction between the OCT and the HCT state is obscured further in our simulations by the presence of an intermediate traffic state where both the OCT-like inhomogeneous part and the HCT-like homogeneous part expand with time. We call this intermediate state the ''mixed congested traffic'' (MCT) state [Fig. 6(a)]. As f_{rmp} increases, the change from the OCT state to the MCT state and then to the HCT state seems to occur in a smooth way. We thus infer that the OCT, MCT, and HCT are different forms of a single jam phase.

We now focus on the HCT state. Notice that even though $f_{up} < f_b$, the area of the congested traffic increases monotonically with the group velocity of the upstream front about -7.68 km/h, which is considerably lower than the usual jam propagation velocity ~ -15 km/h [4]. This monotonic widening of the congested region is caused by the ''blockage'' effect of the ramp, which can be understood easily by recalling that in real highways, a large flux from the on-ramp can almost block the flow of vehicles on main highways. We also mention that the structure of the HCT state is identical to the traffic jam (shock) caused by a blockage [26], which implies that for large f_{rmp}, the ramp works as a bottleneck.

Interestingly, the density in the congested region lies in the linearly unstable region of the homogeneous flow, ρ_{c1} ($=\rho_c$) $< \rho < \rho_{c2}$. Hence according to Refs. [14,15], long wavelength fluctuations of even infinitesimal amplitude should grow in this region. In our simulations, we find that small inhomogeneities in the initial state indeed grow to form clusters. These clusters however disappear when they reach the upstream boundary of the congested region and the congested region becomes homogeneous afterwards. This result implies that inside the linearly unstable region, there exists a range of density where the homogeneous flow is *convectively* stable [27] (that is, the instability drifts away in one particular direction leaving the regions behind unaffected). The same observation is made in Ref. [21], where the HCT state is related to the stationary synchronized flow. As mentioned in the preceding subsection, however, the density-flow relation in the congested region of the HCT state lies on the single curve $(\rho, \rho V(\rho))$, which differs from the experimental observations of scattered data [3]. We mention that the HCT state may be very sensitive to the presence of noises since it is only convectively stable.

It is instructive to compare the stability ranges in Fig. 1(c) with those in Fig. 1(b). The stability range of the SLC state lies entirely below f_{rmp}^b in Fig. 1(c) while it is mostly above f_{rmp}^b in Fig. 1(b). Also the stability range of the OCT reaches below f_{rmp}^b in Fig. 1(c) while it lies entirely above f_{rmp}^b in Fig. 1(b). This suggests that when the sum $f_{up} + f_{rmp}$ is the same, the formation of the cluster is easier for larger f_{rmp} and thus the actual total flux level in the downstream is lower. Physi-

cally this tendency can be understood as resulting from the larger density gradient near the on-ramp when the relative portion of f_{rmp} is larger. This trend is indeed observed in highway measurements [28] and is called the ''capacity reduction.''

III. ANALYTIC SOLUTIONS OF THE SLC AND THE HCT STATES

In Sec. II, we showed that various forms of traffic flows occur near an on-ramp. In the case of the free flow and the usual traffic jam, they are affected by the on-ramp in minor ways and their properties are essentially the same as those without an on-ramp, which have already been investigated intensively [15]. For other phases, however, the presence of the on-ramp is crucial and understanding of their properties are relatively poor. In this section, we present analytic studies of two forms of traffic flow, the SLC state and the HCT state.

A. Standing localized cluster (SLC) state

The analytic examination of the SLC state is relatively simple since all time dependence disappears. This analysis also provides a good starting point for future analysis of the RH state and the OCT state since they are closely related to the SLC state as discussed in the preceding section. Hence we present below the analysis of the SLC state in detail.

In a homogeneous highway, inhomogeneities in the density or the velocity always propagate. In the presence of an on-ramp, on the other hand, the numerical investigation in the previous section shows that inhomogeneities may form a *standing* cluster without propagation. Here we demonstrate analytically that the model [Eqs. (1) and (2)] indeed allows standing cluster solutions in the presence of an on-ramp.

To obtain the SLC solution, one imposes

$$\frac{\partial \rho}{\partial t} = \frac{\partial v}{\partial t} = 0. \tag{5}$$

By integrating Eq. (1) with respect to x, one obtains

$$\rho(x)v(x) = f_{rmp} \int_{-\infty}^{x} \varphi(x)dx + f_{up} \equiv q(x). \tag{6}$$

Since the function $q(x)$ is completely determined for given f_{rmp} and f_{up}, one can use this equation to express $\rho(x)$ in terms of $v(x)$. Using this, one can rewrite Eq. (2) as follows:

$$\mu \frac{d^2v}{dx^2} = q\left(1 - \frac{c_0^2}{v^2}\right)\frac{dv}{dx} - \frac{q(x)}{\tau v}\left[V\left(\frac{q(x)}{v}\right) - v\right] + \frac{c_0^2}{v}q'(x), \tag{7}$$

where $\partial/\partial x$ has been replaced by d/dx since all time dependence disappears.

For further analysis, it is convenient to assume a particular form of the influx profile $\varphi(x)$. We take the localized influx limit and choose $\varphi(x) = \delta(x)$. Then $q(x)$ becomes f_{up} for $x < 0$, $f_{up} + f_{rmp}$ for $x > 0$, and $q'(x) = f_{rmp}\delta(x)$. Then Eq. (7) can be decomposed into two separate problems defined on two semi-infinite regions, $x < 0$ and $x > 0$, with the matching conditions at $x = 0$,
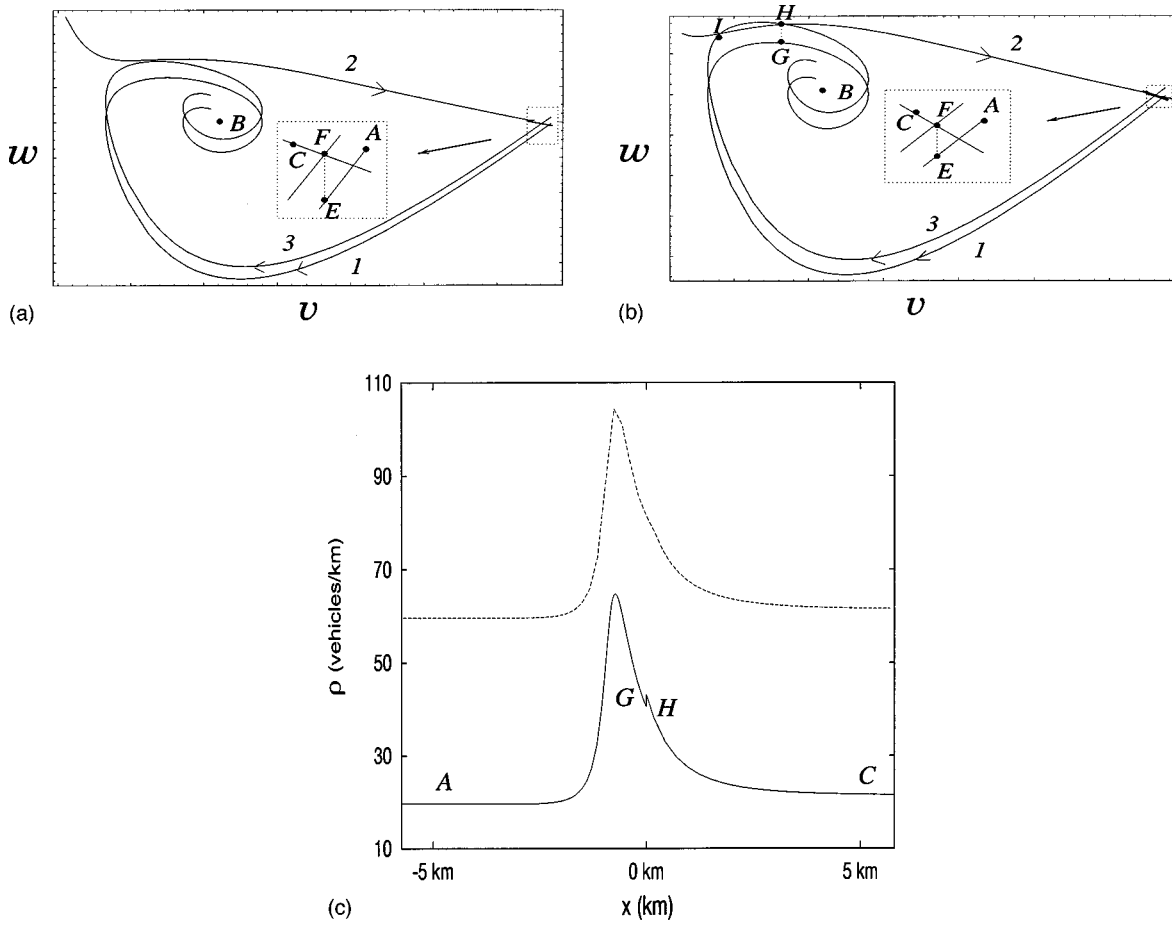
FIG. 7. The flow in the phase space (v,w) (a) with f_{rmp} slightly below the lower stability limit of the SLC state and (b) with f_{rmp} slightly above the lower stability limit. The path 1 represents the flow that is associated with the unstable eigendirection of the fixed point $(v_{n1},0)$ (point A), and the path 2 the flow that is associated with the stable eigendirection of the fixed point $(v_{rmp1},0)$ (point C). The path 3 represents the image of the path 1 through the mapping (8). The insets are the enlargements of the dotted regions at right. (c) The density profile (solid line) of the SLC state obtained analytically for $f_{up}= 1948$ vehicles/h and $f_{rmp}= 121$ vehicles/h. The marks A, G, H, C represent corresponding points in Fig. 7(b). The density profile obtained from the numerical simulation of Eqs. (1) and (2) is also given for comparison (dotted line, vertically shifted 40 vehicles/km). Notice that the density jump at the on-ramp $(x=0)$ in the solid line [due to the approximation $\varphi(x)=\delta(x)$] is smoothed out in the dotted line.

$$v(x)|_{x=0+}=v(x)|_{x=0-},$$

$$\left.\frac{dv}{dx}\right|_{x=0+}=\left.\frac{dv}{dx}\right|_{x=0-}+\frac{c_0^2}{\mu v(0)}f_{rmp}. \qquad (8)$$

For each semi-infinite region, it is instructive to rewrite Eq. (7) as follows:

$$\mu\frac{dw}{dx}=q_s\left(1-\frac{c_0^2}{v^2}\right)w-\frac{q_s}{\tau v}\left[V\left(\frac{q_s}{v}\right)-v\right],$$

$$\frac{dv}{dx}=w, \qquad (9)$$

where $s=$p(ositive) for $x>0$ and $s=$n(egative) for $x<0$, and $q_p=f_{up}+f_{rmp}$, $q_n=f_{up}$. Notice that after the variable transformations $v\rightarrow y$, $x\rightarrow t$, $\mu\rightarrow m$, Eq. (9) can be regarded as the equation of motion of a particle subject to a potential $U_s(y)$ where $dU_s/dy=(q_s/\tau y)[V(q_s/y)-y]$ and to the "strange" coordinate-dependent damping force.

For the safe velocity $V(\rho)$ adopted in this paper, Eq. (9) is highly nonlinear and it does not seem feasible to write down solutions in a closed form. However, qualitative properties of the solutions can be still investigated by taking Eq. (9) as a set of flow equations defined on the phase space (v,w).

Since the global structure of the flow is largely determined from properties of fixed points, we first find fixed points of Eq. (9). Simple algebra shows that there are three fixed points, $(v,w)=(0,0),(v_{s1},0),(v_{s2},0)$. The first one is unphysical since $v=0$ implies $\rho\rightarrow\infty$. This unphysical fixed point appears since we set $V(\rho)=0$ for $\rho>\hat{\rho}$, and we ignore this below. The other two come from the two solutions v_{s1}, v_{s2} $(<v_{s1})$ of $V(q_s/v)=v$. [It can be easily verified that for $q_s<f_{max}$, there are always two solutions, the larger one corresponding to the maximum point of the potential $U_s(y)$ and the smaller to the minimum point.]

We are interested in the solutions where

$$v(x)\rightarrow\begin{cases} v_{n1} & \text{for } x\rightarrow-\infty \\ v_{p1} & \text{for } x\rightarrow\infty. \end{cases} \qquad (10)$$

Thus $(v_{n1},0)$ [point A in Figs. 7(a) and 7(b)] is the relevant fixed point for $x<0$. By linearizing Eq. (9), it can be verified that it is a saddle point. Then the flow [path 1 in Figs. 7(a) and 7(b)] that is associated with the unstable eigendirection of the fixed point determines the entire flow in the semi-infinite region $x<0$. Similarly $(v_{p1},0)$ [point C in Figs. 7(a) and 7(b)] is the relevant fixed point for $x>0$, which is again a saddle point. The entire flow in the positive semi-infinite region is then determined by the flow [path 2 in Figs. 7(a) and 7(b)] that is associated with the stable eigendirection of the fixed point.

In order to construct a legitimate solution from the path 1 and 2, one should join the two paths using the matching conditions [Eq. (8)]. It is convenient to regard the conditions [Eq. (8)] as a definition of a mapping defined in the phase space (v,w), from a point (v,w) to $(v,w+c_0^2 f_{rmp}/\mu v)$. The effect of the mapping is shown in Fig. 7(a), where the path 1 is mapped to the path 3. The path 3 crosses the path 2 at a point denoted as F in the inset. Then one can construct a full solution by connecting the curve AE with the curve FC. This solution exists for an arbitrary small value of f_{rmp} and represents the free flow solution (with a transition layer [16] at the on-ramp).

Different solutions appear for sufficiently large f_{rmp}. The mapping of the path 1 to the path 3 for a larger f_{rmp} is depicted in Fig. 7(b). Now the path 3 crosses the path 2 at three points F,H,I, which implies the presence of three solutions. The solution associated with the crossing point F again corresponds to the transition layer solution. The two other solutions associated with the crossing points H and I correspond to the desired SLC solutions. Each solution provides the velocity profile for $-\infty<x<\infty$, from which the density profile can be obtained from $\rho(x)=q_s/v(x)$. Figure 7(c) compares the density profile associated with the crossing point H with that from the direct numerical simulation of the traffic model [Eqs. (1) and (2)] with the Gaussian form of $\varphi(x)$. Notice that the two profiles are essentially identical except for a small difference in the ramp region, which arises due to the approximation of the input flux profile by a delta function. The density profile associated with the crossing point I can be obtained in a similar way. This solution, however, is not found in the direct numerical simulation, which suggests that this solution is linearly unstable.

This analysis implies that the SLC solutions appear only for f_{rmp} larger than a critical value. Precisely at the critical value, the two crossing points H and I coincide. For f_{rmp} larger than the critical value, numerical simulations indicate that only one solution (one through the crossing point H) is stable and the other is not. Thus one finds that a turning point connecting the stable and unstable SLC solutions appear at the critical ramp flux.

Above considerations use a specific form of an influx profile. We believe that the precise profile does not change the qualitative nature of above discussion. In fact, the value of the critical ramp flux for the SLC state obtained using the approximation $\varphi(x)=\delta(x)$ is found identical within the numerical accuracy to that obtained from the direct numerical simulation of Eqs. (1) and (2) [with $\varphi(x)$ Gaussian].

B. Homogeneous congested traffic (HCT) state

When the on-ramp influx is added, we observe another kind of the traffic jam: The downstream front is fixed at the

on-ramp and the upstream front moves with a fixed group velocity. Between the downstream and the upstream fronts, the congested region of the homogeneous flow is maintained [Fig. 6(b)]. We notice that the upstream front is a steady structure in a proper reference frame. Below we show analytically that Eqs. (1) and (2) possess the HCT state solution. Since the congested region is homogeneous, one can split the discussion into two parts, one for the moving upstream front and the other for the fixed downstream front. For the upstream front, the relevant equations of motion are

$$\frac{\partial \rho}{\partial t}+\frac{\partial(\rho v)}{\partial x}=0, \tag{11}$$

$$\rho\left(\frac{\partial v}{\partial t}+v\frac{\partial v}{\partial x}\right)=\frac{\rho}{\tau}[V(\rho)-v]-c_0^2\frac{\partial \rho}{\partial x}+\mu\frac{\partial^2 v}{\partial x^2}. \tag{12}$$

Since this front is surrounded by *wide* regions of the homogeneous flow both in the upstream and the downstream, one can impose the following boundary conditions:

$$\rho(x=-\infty,t)=\rho_-=\rho_{up}, \tag{13}$$

$$v(x=-\infty,t)=v_-=V(\rho_-), \tag{14}$$

$$\rho(x=+\infty,t)=\rho_+, \tag{15}$$

$$v(x=+\infty,t)=v_+=V(\rho_+). \tag{16}$$

Here ρ_- is the density of the far upstream region and ρ_+ of the congested region Also the spatial coordinate is chosen in such a way that $x=+\infty$ corresponds to a location deep in the congested region instead of the far downstream in the original equations (1) and (2).

Let us assume that Eqs. (11) and (12) allow a *steady* state solution that satisfies the boundary conditions Eqs. (13), (14), (15), and (16). Here the steady state means that in a proper reference frame, all time-dependence disappears. We perform the change of the reference frame:

$$x'=x-v_g t, \tag{17}$$

$$t'=t, \tag{18}$$

and neglect all time dependence in this new reference frame to find

$$\frac{dq'}{dx'}=0, \tag{19}$$

$$q'\frac{dv}{dx'}=\rho\frac{V(\rho)-v}{\tau}-c_0^2\frac{d\rho}{dx'}+\mu\frac{d^2 v}{dx'^2}, \tag{20}$$

where $q'\equiv\rho v-\rho v_g$. We can determine the constants q' and v_g from the boundary conditions Eqs. (13), (14), (15), and (16). From the condition that the in-flux to and the out-flux from the front should be the same in the primed reference frame, we obtain

$$v_g=\frac{\rho_+v_+-\rho_-v_-}{\rho_+-\rho_-}, \tag{21}$$

$$q' = \frac{\rho_+ \rho_- (v_- - v_+)}{\rho_+ - \rho_-}. \qquad (22)$$

Using Eq. (19), one has

$$\rho = \frac{q'}{v - v_g}. \qquad (23)$$

Plugging in this expression into Eq. (20), one finds

$$\mu \frac{d^2 v}{dx'^2} + q' \left[\frac{c_0^2}{(v - v_g)^2} - 1 \right] \frac{dv}{dx'} + F(v; q', v_g) = 0, \qquad (24)$$

where

$$F(v; q', v_g) \equiv \frac{q'}{\tau(v - v_g)} \left[V\left(\frac{q'}{v - v_g} \right) - v \right]. \qquad (25)$$

Equation (24) is again an equation of motion of a particle subject to a conservative force $-F$ and the coordinate-dependent damping force. The boundary conditions Eqs. (13) and (14) ensure that $F(v_\pm; q', v_g) = 0$ automatically. Since $v_- > v_+$, the root $v_-(v_+)$ corresponds to the potential maximum (minimum). Thus the nature of the stationary state is clear in the particle motion analogy. At $x = -\infty$, the particle is at the unstable maximum point $v = v_-$. As "time" x increases, the particle slides down the hill and after some time, it settles down at $v = v_+$ due to the friction, provided the damping coefficient in Eq. (24) remains positive. This particle motion describes the upstream front of the HCT state [Fig. 6(b)].

Before we begin the next analysis of the downstream front of the HCT state [Fig. 6(b)], one remark is in order. In the direct numerical simulation of Eqs. (1) and (2), the vehicle velocity in the congested region of the HCT state is fixed for given $f_{\rm up}$ and $f_{\rm rmp}$. However, in the above analysis of the upstream front, where $f_{\rm up}$ is used to fix $v_- = v_{\rm up}$, the value of v_+ is still a free parameter. We show below that this degree of freedom should be used to allow the downstream front solution.

Analysis of the stationary downstream front is very similar to the analysis of the SLC state in the preceding subsection. Using the condition of the stationarity and integrating Eq. (1), one obtains Eq. (5) and (6), respectively. Adopting the approximation $\varphi(x) = \delta(x)$, one recovers the matching conditions at the ramp [Eq. (8)] and the set of the flow equations [Eq. (9)]. The value of q_n should be $\rho_+ v_+$ to allow a continuous connection of $v(x)$ to the upstream front solution and $q_p = q_n + f_{\rm rmp}$. The asymptotic behavior of $v(x)$ far away from the on-ramp should be chosen differently as follows:

$$v(x) \to \begin{cases} v_{n2} = v_+ & \text{for } x \to -\infty \\ v_{p1} & \text{for } x \to \infty, \end{cases} \qquad (26)$$

where v_{p1} and v_{n2} are defined in the same way as in the preceding subsection, and $x \to -\infty$ corresponds to the region deep in the congested region.

Notice that for $x \to -\infty$, $v(x)$ approaches v_{n2} instead of v_{n1} since v_+ corresponds to the smaller of the two solutions
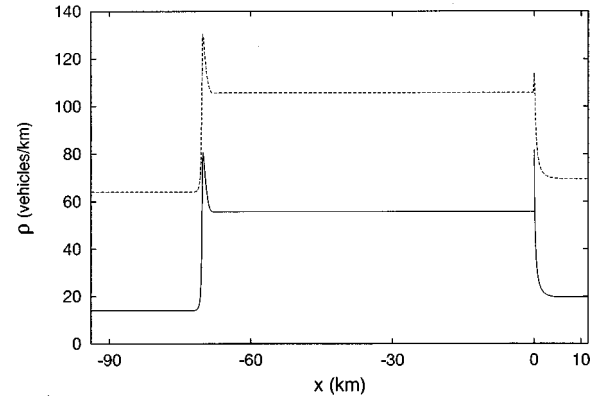

FIG. 8. The density profile of the HCT state obtained analytically (solid line) under the approximation $\varphi(x) = \delta(x)$ for $f_{\rm up} = 1497$ vehicles/h and $f_{\rm rmp} = 762$ vehicles/h. The density profile obtained from the numerical simulation of Eqs. (1) and (2) is also given for comparison (dotted line, vertically shifted 50 vehicles/km). Small differences between the two are due to the different choices of $\varphi(x)$.

of $V(q_n/v) = v$ (or since the corresponding density ρ_+ lies on the descending slope of the homogeneous density-flow relation). This difference in the asymptotic behavior results in a qualitative change. It can be verified through the linearization of Eq. (9) that $(v_{n2}, 0)$ is a *stable* fixed point. Then we find $v(x) = v_{n2}$ for the entire semi-infinite region $x < 0$, which should be contrasted to the preceding subsection. Near the fixed point $(v_{p1}, 0)$, on the other hand, the situation is similar to the preceding subsection and the flow in the positive semi-infinite region becomes a continuous path, like the path 2 in Figs. 7(a) and 7(b).

To construct a full solution of the HCT downstream front, the separate solutions for $x < 0$ and $x > 0$ should be joined using the matching condition [Eq. (8)]. Since the velocity for $x < 0$ is constant, the matching conditions reduce to

$$v(x)|_{x=0+} = v_{n2},$$

$$\left. \frac{dv}{dx} \right|_{x=0+} = \frac{c_0^2}{\mu v(0)} f_{\rm rmp}. \qquad (27)$$

This matching conditions can be satisfied only when the phase space trajectory for $x > 0$ passes the point $(v_{n2}, (c_0^2/\mu v_{n2}) f_{\rm rmp})$. For given v_{n2} and $f_{\rm rmp}$, the path in general does *not* pass the point except for a particular value of $v_{n2} = v_+$. This tuning thus fixes the free parameter v_+ as mentioned before. In general, v_+ is a function of the influx profile $\varphi(x)$ since the matching conditions depend on $\varphi(x)$.

Figure 8 shows the density profile (solid line) of the HCT state obtained from this matching method for $\varphi(x) = \delta(x)$. It is essentially identical to the profile (dotted line) obtained from the numerical simulation of Eqs. (1) and (2), except for the larger density peak at the on-ramp caused by the approximation $\varphi(x) = \delta(x)$. We confirm from the simulation result that the group velocity of the moving front is consistent with -7.68 km/h which is given by Eq. (21) and the damping coefficient $q'[c_0^2/(v - v_g)^2 - 1]$ is positive in the congested region.

IV. CONCLUSION

The traffic equation with a source term representing the on-ramp influx of a highway displays a variety of traffic flow states not present in the homogeneous equations. To understand the role of the source term, we map out the phase diagram using the continuum traffic model [Eqs. (1) and (2)] proposed by Kerner and Konhäuser [14]. In our numerical simulation, we use the open boundary condition, which allows one to handle the single on-ramp without using very large system sizes. Due to the possible presence of multiple metastable states, detailed simulation is carried out for a limited number of representative values of the upstream flux f_{up} and for the whole range of the on-ramp flux f_{rmp}. Various traffic states are identified and characterized. The phase diagrams thus obtained are summarized in Fig. 1. It is found that an inhomogeneous but stationary traffic state (SLC) can appear near the on-ramp due to f_{rmp}. This state is related to the recent measurement of the homogeneous synchronized flow. The on-ramp also generates another kind of traffic jam,

which can appear even below the stability limit of the usual traffic jam in homogeneous highways. The structure of this traffic jam varies qualitatively with f_{rmp}. The capacity reduction due to f_{rmp} is also observed. In a certain range of f_{rmp}, the free flow, the RH state, and the traffic jam can all coexist so that the free flow can undergo phase transitions either to the RH state or to the traffic jam state. Analytic investigations are also performed and two nontrivial solutions of Eqs. (1) and (2) are found. These solutions describe the SLC state and the HCT state.

[1] I. Treiterer and J. A. Myers, in *International Symposia on Transportation and Traffic Flow*, edited by D. J. Buckley (A. H. & A. W. Reed Pty Ltd., New South Wales, 1974); M. Koshi, M. Iwasaki, and I. Ohkura, in *Proceedings of the Eighth International Symposium on Transportation and Traffic Theory*, edited by V. F. Hurdle, E. Hauer, and G. N. Stewart (University of Toronto Press, Toronto, Ontario, 1983).

[2] B. S. Kerner and H. Rehborn, Phys. Rev. Lett. **79**, 4030 (1997).

[3] B. S. Kerner and H. Rehborn, Phys. Rev. E **53**, R4275 (1996); B. S. Kerner, Phys. Rev. Lett. **81**, 3797 (1998).

[4] B. S. Kerner and H. Rehborn, Phys. Rev. E **53**, R1297 (1996).

[5] D. Helbing, Phys. Rev. E **55**, 3735 (1997).

[6] D. E. Wolf, M. Schreckenberg, and A. Bachem, *Traffic and Granular Flow* (World Scientific, Singapore, 1996).

[7] M. Schreckenberg and D. E. Wolf, *Traffic and Granular Flow '97* (Springer, Singapore, 1998).

[8] M. Bando, K. Hasebe, A. Nakayama, A. Shibata, and Y. Sugiyama, Phys. Rev. E **51**, 1035 (1995).

[9] K. Nakanishi, K. Itoh, Y. Igarashi, and M. Bando, Phys. Rev. E **55**, 6519 (1997).

[10] K. Nagel and M. Schreckenberg, J. Phys. I **2**, 2221 (1992).

[11] M. Schreckenberg, A. Schadschneider, K. Nagel, and N. Ito, Phys. Rev. E **51**, 2939 (1995).

[12] I. Prigogine and R. Herman, *Kinetic Theory of Vehicular Traffic* (Elsevier, New York, 1971).

[13] D. Helbing, Phys. Rev. E **53**, 2366 (1996).

[14] B. S. Kerner and P. Konhäuser, Phys. Rev. E **48**, R2335 (1993).

[15] B. S. Kerner and P. Konhäuser, Phys. Rev. E **50**, 54 (1994).

[16] B. S. Kerner, P. Konhäuser, and M. Schilke, Phys. Rev. E **51**, 6243 (1995).

[17] S. Krauss, P. Wagner, and C. Gawron, Phys. Rev. E **55**, 5597 (1997).

[18] B. S. Kerner, S. L. Klenov, and P. Konhäuser, Phys. Rev. E **56**, 4200 (1997).

[19] H. Y. Lee, H.-W. Lee, and D. Kim, Phys. Rev. Lett. **81**, 1130 (1998).

[20] D. Helbing and M. Treiber, Phys. Rev. Lett. **81**, 3042 (1998).

[21] D. Helbing, A. Hennecke, and M. Treiber, e-print cond-mat/9809324.

[22] R. Kühne and P. Michalopoulos, in *Traffic Flow Theory*, edited by N. Gartner, C. Messer, and A. Rathi (Transportation Research Board, Washington, D.C., in press).

[23] W. H. Press, B. P. Flannery, S. A. Teukolsky, and W. T. Vetterling, *Numerical Recipes in C* (Cambridge University Press, Cambridge, England, 1988).

[24] The form of $V(\rho)$ is chosen so as to be consistent with the available free flow data [2] and also with large density asymptotic behaviors. But its precise form is not important.

[25] E. A. Jackson, *Perspectives of Nonlinear Dynamics* (Cambridge University Press, Cambridge, England, 1989), Vol. 1.

[26] S. A. Janowsky and J. L. Lebowitz, J. Stat. Phys. **77**, 35 (1994).

[27] P. Manneville, *Dissipative Structures and Weak Turbulence* (Academic Press, New York, 1990).

[28] F. I. Hall and K. Agyemang-Duah, in *Transportation Research Record 1320* (Transport Research Board, Washington, DC, 1991).